# Thick carbon deposition by cascaded arcs

# THICK CARBON DEPOSITION BY CASCADED ARCS

CARBON MATERIALS SPECIAL

**KEYWORDS:** *carbon deposition, cascaded arc, protective coatings*

AD J. M. BUURON, SJAAK J. BEULENS, RIES J. F. van de SANDE, and DANIEL C. SCHRAM
*Eindhoven University of Technology, Department of Physics*
*P.O. Box 513, 5600 MB Eindhoven, The Netherlands*

JAAP G. van der LAAN
*Netherlands Energy Research Foundation (ECN)*
*P.O. Box 1, 1755 ZG Petten, The Netherlands*

Received September 25, 1990
Accepted for Publication December 3, 1990

*An expanding cascaded arc plasma is used for the deposition of different types of carbon layers at high growth rates. Single diamond crystals of 60 μm and 25-μm-thick continuous films are deposited within 1 h on areas of ~3 cm². In recent experiments, pyrolytic graphite films have been deposited. Films up to 200 μm thick have been produced within 20 min on an area of ~12 cm². The film type and growth rate depend on the choice of the optimum reactor parameter settings. To maximize the growth rate and crystallinity of the film, the reactor settings are varied. High growth rates (maximum of 762 nm/s) have been obtained at high temperatures (600 to 1000°C). Several diagnostic techniques are used to analyze the film. The purity of the films has been confirmed by Auger electron spectroscopy.*

## INTRODUCTION

During the last decades, many different types of discharges have been used for plasma surface modification, etching, and deposition. The most recent method is the application of a low-pressure radio-frequency or dc glow discharge.[1] In this method, the substrate is immersed in an argon/hydrocarbon plasma and the deposition process is governed by diffusion. The deposition rates are relatively low, of the order of 1 to 20 μm/h.

In 1981, the flowing cascaded arc was introduced as a powerful particle source.[2] Hydrocarbon monomer gas can effectively be dissociated in CH radicals and excited and ionized carbon particles. Combined with the supersonic expansion of the plasma into a vacuum chamber toward the substrate, deposition rates of hundreds of nanometres per second have been reached for amorphous hydrogenated carbon (a-C:H) films. The main feature of the method is the separation of the three functions of production, transport, and deposition. The type, quality, and growth rate of the films can be controlled by varying the reactor parameters. The growth rate can be raised by increasing the flux of active particles on the substrate, e.g., by increasing the arc power. With this configuration, very high growth rates (200 nm/s) have been reached for amorphous carbon films at low substrate temperatures (20 to 100°C) with argon/$CH_4$ and argon/$C_2H_2$ plasmas (typically at a ratio of 100/1). For higher deposition temperatures and with addition of $H_2$ to the gas flow, the growth rate is strongly reduced.[3,4] Diamond films have been deposited at 1000°C in an argon/hydrogen environment (50/50 ratio) at a rate of ~10 nm/s. The main factors determining the crystallinity of the film are the substrate temperature and the amount of hydrogen admixture in the argon flow.

The growth rate, the refractive index, and the thickness of the film are monitored *in situ* with helium-neon (He-Ne) ellipsometry.[2] *Ex situ*, the layers are analyzed by a number of techniques. Ultraviolet-visible infrared spectroscopic ellipsometry[5] gives information on the band gap, the absorption bands (presence and type of carbon-hydrogen bonds), and the refractive index. Raman scattering is applied to determine the carbon-carbon bond type and the degree of crystallinity in the film. Information on the morphology is also obtained by scanning electron microscopy (SEM). Additional techniques are electron spectroscopy for chemical analysis to determine the type of film, Rutherford backscattering to determine hydrogen content and depth profile, low-energy electron diffraction to determine crystallinity, and Auger electron spectroscopy to determine impurities.

In a joint effort among Eindhoven University of Technology, the Netherlands Energy Research Foundation, and the Next European Torus (NET) team, a feasibility study is being performed on the possibility

of *in situ* repair of erosion damage on divertor plates in NET (Ref. 6) by means of fast carbon deposition by a cascaded arc. Graphitic or diamondlike layers may be particularly suitable candidates because of their high thermal conductivity and shock resistance and their mechanical strength. Deposition experiments with a variety of plasma and deposition parameter settings have been carried out based on the experience acquired during the amorphous carbon and diamond deposition experiments. A brief survey of these earlier projects is given first.

## EXPERIMENTAL CONFIGURATION

The reactor and the cascaded arc are described in detail elsewhere.[2] Figure 1 shows a schematic of the arc. The arc consists of three cathodes, a stack of ten insulated copper plates, and an end plate with a ring-shaped copper anode, the nozzle. Only one cathode is shown in Fig. 1; the other two are situated circumferentially at 120-deg angles to each other. The components are all water cooled. The cathodes are 1-mm-diam tungsten thorium tips for currents up to 30 A/cathode. The cascade plates have a 4-mm inner bore and are 5 mm thick. Together with the 1-mm-thick insulation plates, they form a 60-mm-long plasma channel. The carrier gas argon is injected at a pressure of 0.5 bar at the beginning of the arc channel at room temperature at a flow rate of typically 100 $cm^3/s$. The electron temperature is approximately constant in the axial direction and is ~15 000 K for standard operating conditions (arc current of 50 A). The heavy particle temperature reaches ~12 000 K in the middle of the arc channel and decreases slightly again toward the exit of the channel.[7] The ionization degree is typically ~10%, rendering an electron density of $\sim 10^{22}/m^3$. Hydrogen can be added at the middle of the channel. To prevent obstruction of the arc channel by graphite formation, the monomer gas is injected through the nozzle at the end of the anode. The cathodes can be inspected through the viewing port.

The position of the cascaded arc in the vacuum chamber is shown in Fig. 2. A movable sample support with an additional sample pedestal is mounted opposite the arc. The plasma mixture is extracted into the vacuum vessel. Consequently, a beam of ions and electrons (10%), atoms, and radicals (argon, carbon, hydrogen, and CH) emerges, directed toward the substrates on the sample support.

Three regions can be distinguished in this expanding beam. In region I, the particles are accelerated to supersonic velocities (~4000 m/s). During this expansion, the electron and the heavy particle temperatures decrease to ~4000 K, and the electron density decreases strongly to $\sim 10^{19}/m^3$. At a distance of ~10 cm from the nozzle (depending on the chamber pressure), a shock (region II) exists, and the temperatures and the electron density rise again to ~8000 K and typically $10^{20}/m^3$, respectively. A carbon ion flux of typically

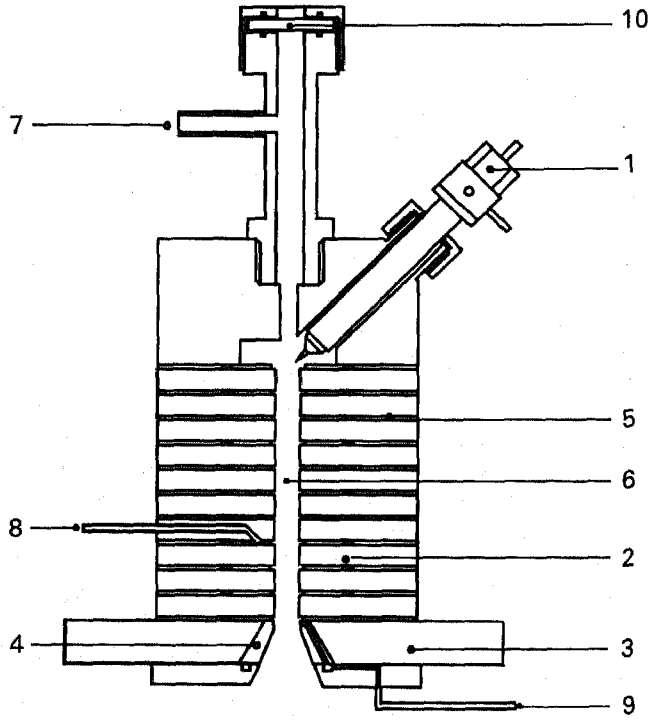


Fig. 1. Schematic of the cascaded arc: (1) cathode, (2) copper plates, (3) end plate, (4) nozzle, (5) insulation plate, (6) plasma channel, (7) argon injection site, (8) hydrogen injection site, (9) monomer injection site, and (10) viewing port.

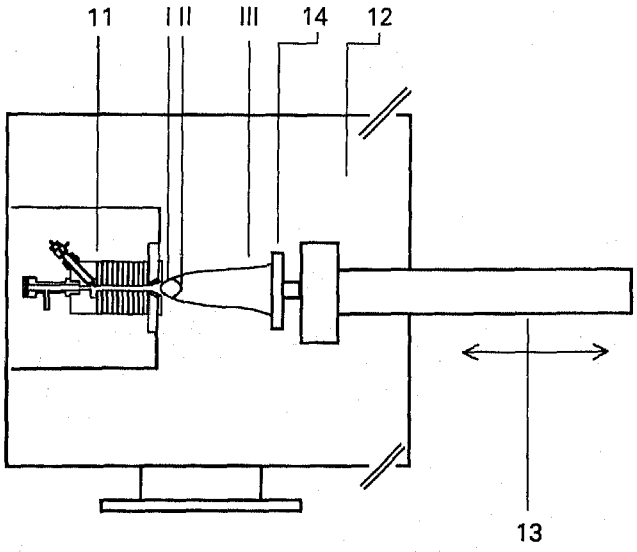


Fig. 2. Schematic of the deposition reactor: (11) position of the arc in the vacuum chamber, (12) vacuum chamber, (13) movable sample support, and (14) sample pedestal.

$8 \times 10^{18}$/s is obtained through charge-exchange with the argon ions. Beyond the shock (region III), the plasma expands subsonically and the plasma composition remains constant ("frozen"). The temperatures drop to ~2000 to 4000 K. The particles are transported further toward the substrate at subsonic velocities.

On the addition of the monomer gas, the plasma cools, and the power and flow settings must be adjusted to avoid "overloading," i.e., incomplete dissociation of the monomer into active CH and carbon species. A typical value for the monomer flow is 1% of the argon flow. Chamber pressure is variable from 0.1 to 100 mbar, the nozzle-to-sample distance from 2 to 80 cm.

## DIFFERENT TYPES OF CARBON DEPOSITS

As pointed out earlier, there is a direct relationship between the different reactor settings and the type and growth rate of the film. To characterize this relationship, the following parameters (and definitions) are of interest:

1. the power product, $P$ = arc power × argon flow rate (W·cm$^3$/s)
2. the monomer flow rate, [$C_xH_y$] (cm$^3$/s)
3. the type of monomer feed gas ($CH_4$, $C_2H_2$, or $C_7H_8$)
4. the inverse energy factor, $Q$ = carbon flow rate/$P$ (W$^{-1}$)
5. the hydrogen flow rate, expressed as the hydrogen-carbon (H/C) ratio
6. the chamber pressure, $p_c$ (mbar)
7. the substrate temperature, $T_s$ (°C)
8. the nozzle-to-sample distance, $d_{n\text{-}s}$ (cm).

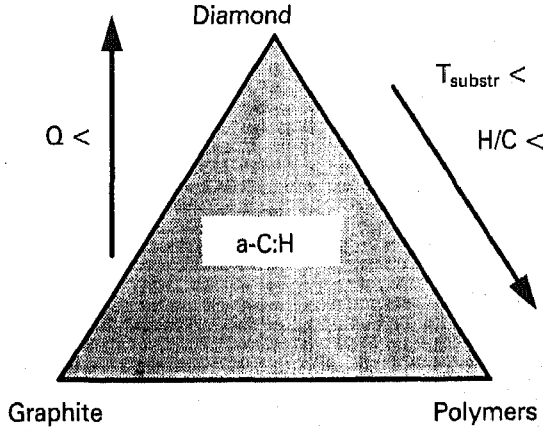


Fig. 3. Relationship between film type and deposition parameters.

The growth rate is a function of all of these parameters.

For the film type, parameters 4, 5, and 7 are of particular interest. This dependence may be summarized in Fig. 3. The inner part of the triangle represents the whole spectrum of possible a-C:H compounds. With an increasing H/C ratio in the beam and an increasing substrate temperature, the hydrogen content in the film tends toward zero, resulting in the limiting cases of graphite and diamond. The hydrogen radicals in the beam etch away hydrogen atoms from carbon-hydrogen bonds. Under specific conditions, the radicals etch graphitic carbon-carbon bonds so that diamond may be obtained. In the case of low $T_s$ and a beam H/C ratio of zero, a polymerlike film with high hydrogen content (>60%) is formed.

The reactor settings for some specific deposits are summarized in Table I. The values for graphite should be considered as indications based on experiences acquired during the diamond deposition experiments.[4] The $Q$ factor for diamond is not defined because of the large amount of hydrogen admixture.

### a-C:H Films

In Fig. 4, some of the properties of a-C:H films, obtained at room temperature, are shown as a function of $Q$. Steel samples with a thin (2-$\mu$m) gold layer were used as a substrate. This facilitates monitoring of the refractive index and the film thickness by *in situ* He-Ne ellipsometry.[2] The optical bandgap was determined using spectroscopic ellipsometry by way of a Tauc plot.[5] Furthermore, the presence of hydrogen in $CH_2$ and $CH_3$ binding forms was also observed from the carbon-hydrogen absorption bands. The total hydrogen content was estimated to be in the 10 to 60%

TABLE I

Typical Parameter Settings for a-C:H, Diamond, and Graphite Deposition

| | a-C:H | Diamond | Graphite |
|---|---|---|---|
| Argon flow (cm$^3$/s) | 100 | 20 | 100 to 150 |
| Monomer flow (cm$^3$/s) | 1.8 | 0.2 | 1 to 8 |
| Molecular hydrogen flow (cm$^3$/s) | 0 | 20 | 0 to 15 |
| Arc current (A) | 50 | 35 | 35 to 50 |
| Arc voltage (V) | 88 | 110 | 74 to 100 |
| Arc power (kW) | 4.4 | 3.85 | 2.5 to 5 |
| $Q$ ($10^{-6}$ W$^{-1}$) | 4.1 | --- | >4 |
| H/C ratio | 0 | 100 | <5 |
| $T_s$ (°C) | 20 | 1000 | 400 to 800 |
| $d_{n\text{-}s}$ (cm) | 80 | 5 | 20 to 40 |
| $p_c$ (mbar) | 1 | 60 | 1 to 10 |

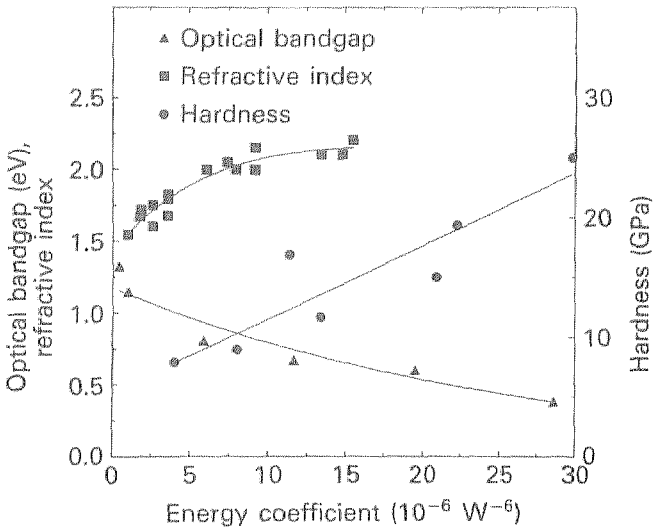


Fig. 4. Optical bandgap, hardness, and refractive index of a-C:H films as a function of $Q$.

range for films with refractive indexes between 1.3 and 2.2. The hardness of the films increases strongly with increasing $Q$, from 400 Vickers for polymerlike to 5000 for diamondlike films.[8] Note that, for graphite deposition (bandgap of 0 eV, refractive index of 2.18), the $Q$ factor may have to be high.

The maximum deposition rate achieved is 200 nm/s on an area of ~100 $cm^2$. The film morphology as shown in Fig. 5a does not reveal any distinct features. The Raman spectrum (Fig. 5b) exhibits the typical continuous bulk signal for a film of noncrystalline nature.[9]

### Diamond

In the past, single diamond crystals and films were produced in a collaborative effort with Philips Aachen.[4] The deposition conditions used are given in Table I. Three-inch silicon wafers were used as the substrate. The substrate was heated by the plasma beam itself. The substrate temperature was monitored with an optical pyrometer. Without special pretreatment of the surface, individual faceted crystals of 15 to 25 $\mu$m (up to a maximum of 65 $\mu$m) were deposited within 1 h (Fig. 6a). If the substrate surface is pretreated by scratching with diamond powder (1-$\mu$m particles), continuous diamond films were grown on an area of ~3 $cm^2$ (Fig. 6b). The number of nucleation sites is strongly increased in this case as a consequence of the surface roughness.

For the individual crystals as well as for the continuous film, the structures are well faceted only in the center of the deposit. Raman spectroscopy reveals that, in both cases, the morphology changes from diamond to graphitic ball-shaped and amorphous structures near the edges of the substrate. This is caused by a combination of three factors: a reduced substrate temperature near the edge, a different effective pressure as a consequence of the flow pattern, and a change in particle densities. In Fig. 7, some Raman spectra are shown. It is clearly demonstrated that moderate chamber pressures can lead to the deposition of graphitic material.

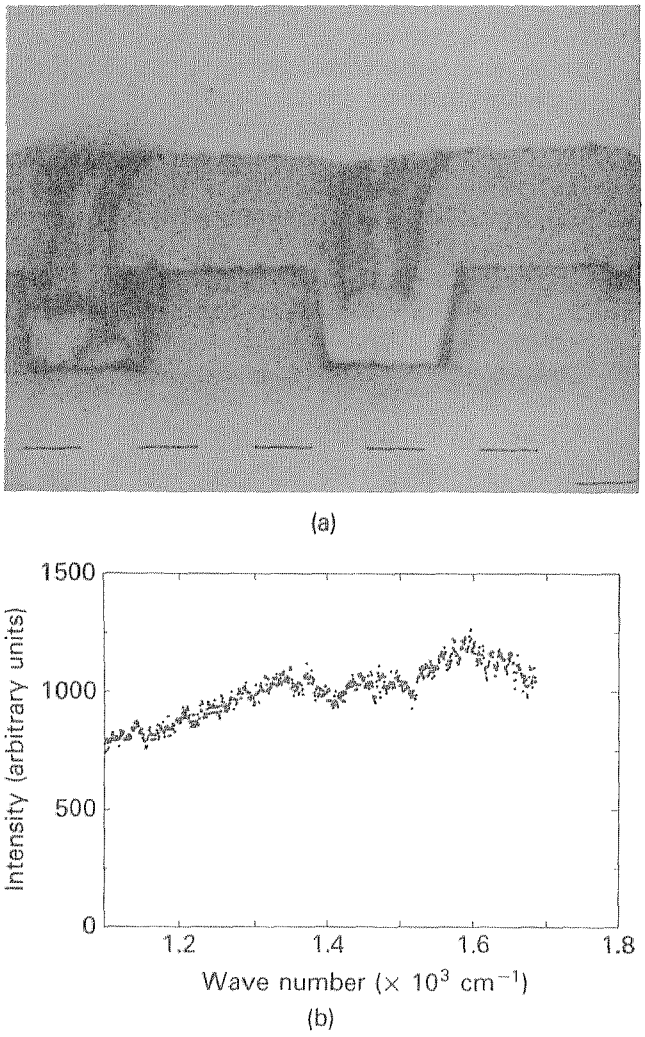


Fig. 5. (a) SEM image of trenches filled with an a-C:H film (1 bar corresponds to 1 $\mu$m) and (b) Raman spectrum of the film.

## GRAPHITE DEPOSITION

In the next-step fusion device NET/International Thermonuclear Experimental Reactor (ITER), the materials for the plasma-facing components are a critical issue. Of most concern is the design of the divertor, which will receive a peak heat flux of 15 $MW/m^2$ during normal operation. The divertor surface will reach temperatures up to 1000°C and suffer from the effects of

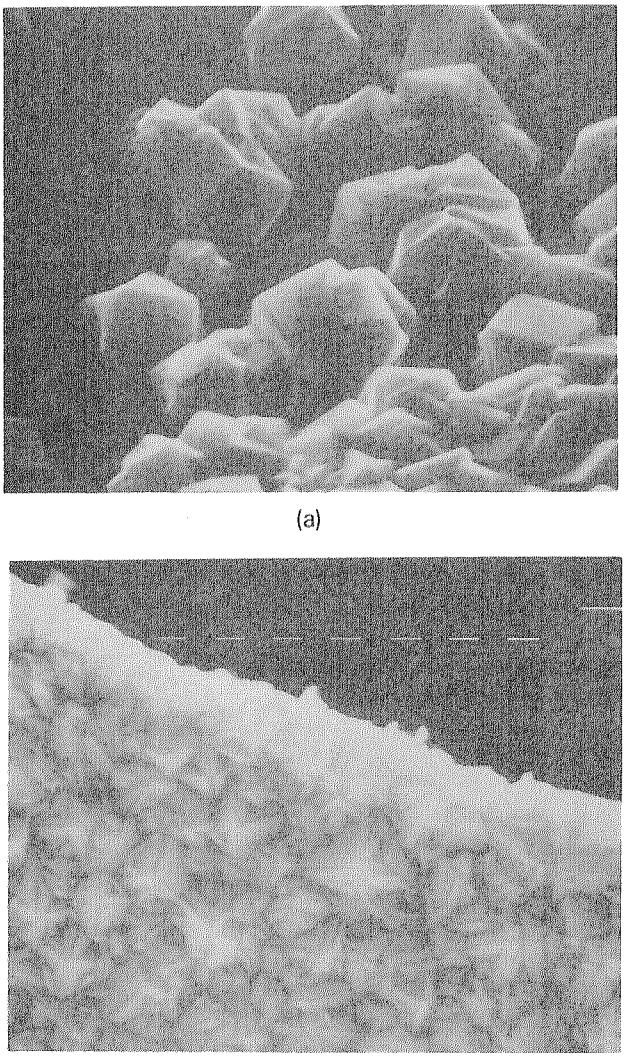

(a)

(b)

Fig. 6. SEM image of (a) individual diamond particles (1 bar represents 10 $\mu$m) and (b) a continuous diamond film (1 bar corresponds to 1 $\mu$m).

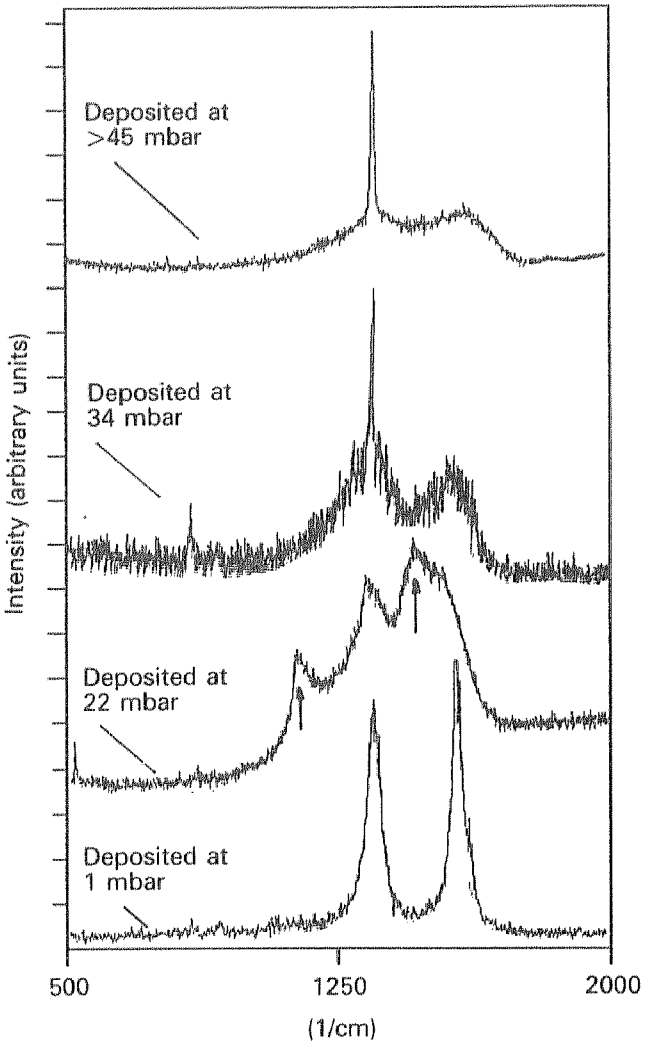


Fig. 7. Raman spectra of deposits obtained under the diamond conditions (Table I), with variable chamber pressure. At 1 mbar, only the peaks associated with graphitic material can be observed. From 22 mbar on, the diamond precursor peaks at $\pm 1150$ and $\pm 1470$ cm$^{-1}$ appear, and then the single crystal diamond peak at 1332 cm$^{-1}$ becomes predominant.

severe disruptions with peak energy dumps of 20 MJ/m$^2$ within milliseconds.[6] Disruption erosion is a primary lifetime-determining factor. Covering the divertor plates with either pyrolytic carbon (PyC) or carbon-fiber composite (CFC) is considered one of the best engineering solutions. Recent estimates for the erosion of a carbon divertor indicate values of 0.5 to 1 mm of material loss per disruption event.[10] Avoiding frequent shutdown of the machine for replacement of the plates is a major problem.

Graphitic or diamondlike carbon deposition by cascaded arc gun is an option for *in situ* repair of erosion damage. The primary requirements for the coating to be deposited are that it should be crystalline (good thermomechanical performance) and that the deposition rate should be high [thick (several millimetres) layers within acceptable periods of time]. As a first research stage, a program of reactor settings, starting from the graphite values of Table I, has been attempted in which increasing the growth rate is emphasized.

### Specific Experimental Data

All the experiments were performed with the setup shown in Fig. 1. The desired deposition temperature was attained by direct heating of the substrate by the plasma beam itself. The sample holder consisted of a hollow stainless steel cylinder with an auxiliary heating facility up to 500°C. A stainless steel (AISI 316 Ti)

pedestal with a sample support was mounted on this. The head could be screwed on the pillar. The dimensions of this pedestal were chosen so that an extensive range of substrate temperatures from 400 to 1200°C could be covered on different substrate-to-sample distances. The cross section of the top disk was 6 cm; the 1-cm long pillar had a 1.5-cm cross section. A Cr-Al thermocouple for temperature measurements was mounted right next to the sample. Surface temperatures were also measured by an optical pyrometer (a Chino IR-AHIS). A water-cooled sample holder was used for deposition experiments at 100°C.

As substrates, 10-mm disks (5 mm thick) of CFC (Dunlop DMS-678) were used. Experiments with the fiber planes parallel and perpendicular to the surface normal were carried out. As a reference for weight gain determination and for morphology considerations, experiments were also executed with samples of commercial graphite and stainless steel (AISI 316 Ti).

The graphitic samples were baked at 200°C for 24 h. They were preheated to a temperature of 600°C by an $Ar/H_2$ plasma (100:5 ratio) in 20 min in the deposition reactor. As feed gases, $CH_4$ and $C_2H_2$ were used. To encourage the deposition of a crystalline layer rather than an amorphous hydrogen-containing layer, several experiments were done with different amounts of hydrogen added. Observations for morphology were done by SEM. The crystallinity of the layer was determined by Raman spectroscopy. Film thickness and growth rate were determined by weight change measurements.

## Results and Discussion

For convenience, we introduce the following quantities and notations:

$P'$ = normalized power product: $P' = P/P_s$, where $P_s$ is the power product at the following standard settings: $I_{arc} = 35$ A, $V_{arc} = 74$ V, argon flow = 100 cm$^3$/s. It follows that $P_s = 2.59 \times 10^5$ cm$^3 \cdot$kW/s.

$Q'$ = normalized energy coefficient: $Q' = Q/Q_s$, where $Q_s$ is the $Q$ factor for a flow of 1 cm$^3$/s $CH_4$. At the standard power product $P_s$, $Q_s$ has the value $3.86 \times 10^{-6}$ W$^{-1}$.

$R_d$ = growth rate, determined from weight measurements, assuming a density of 1 g/cm$^3$. Inaccuracy in $R_d$ by this way of determination is generally <1 nm/s.

$[C_xH_y] = z$ = monomer flow of $z$ cm$^3$/s.

Note that in this experimental configuration, $T_s$ is a function of $d_{n\text{-}s}$, $P$, $p_c$, and, to a minor extent, of the monomer admixture. The growth rate is a function of the substrate temperature.[3] This should be taken into account when considering the results presented below. The main tendencies, however, are not disturbed by this temperature dependence. Furthermore, no definite distinctions between the growth rate results for the parallel and perpendicular CFC samples were observed.

The following results are for films produced at a nozzle-to-sample distance of 20 cm, substrate temperatures between 600 and 1000°C (determined by pyrometry), and with H/C = 0 (no $H_2$ admixture) unless otherwise indicated. In the SEM pictures, 1 bar represents 100 $\mu$m unless otherwise indicated.

### *Growth Rate*

Figures 8 through 11 show the dependence of the growth rate as a function of the relevant deposition parameters. For the initial standard power product

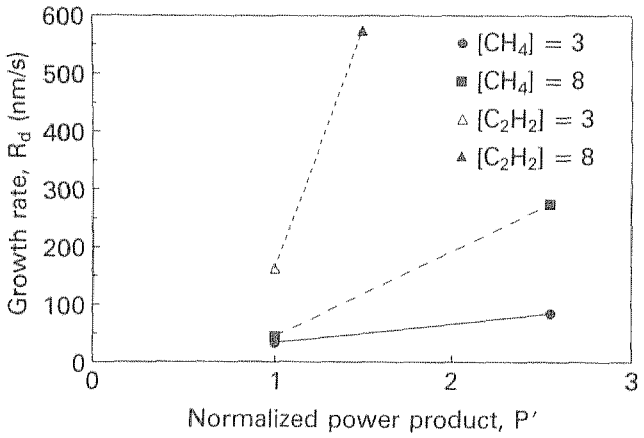


Fig. 8. Deposition rate $R_d$ as a function of normalized power product; $p_c = \frac{8}{3}$ mbar.

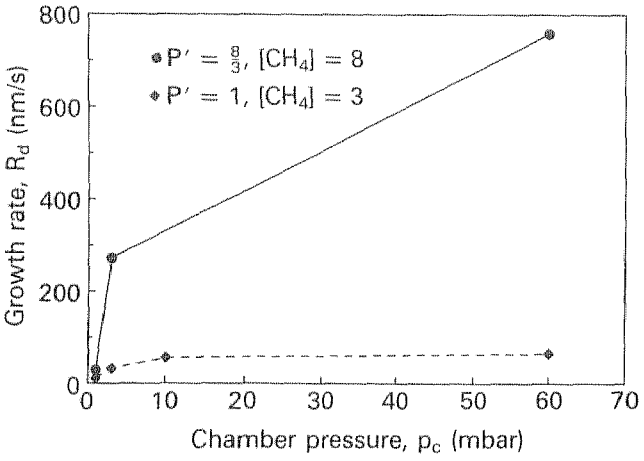


Fig. 9. Deposition rate $R_d$ as a function of chamber pressure.

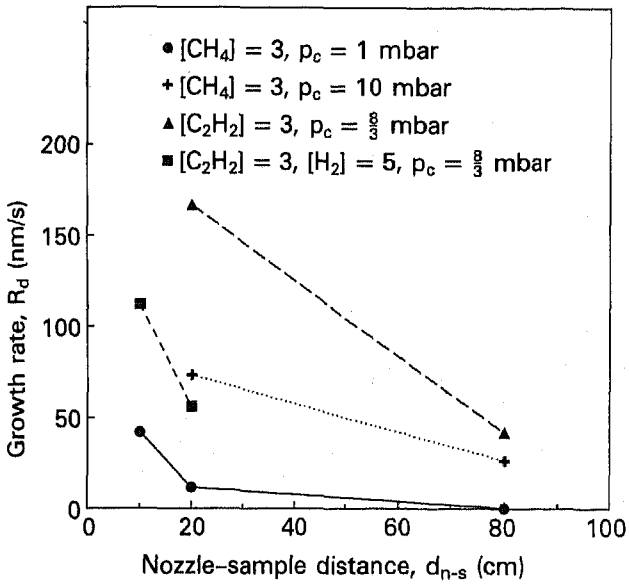


Fig. 10. Deposition rate as a function of nozzle-sample distance: $P' = 1$. (At $d_{n\text{-}s} = 80$ cm, $T_s = 100$°C.)

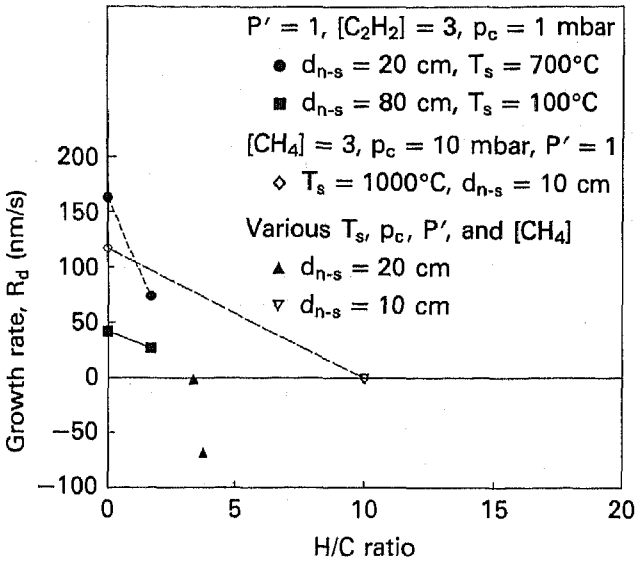


Fig. 11. Deposition rate $R_d$ as a function of H/C ratio in the beam.

($P' = 1$), saturation arises readily at low $CH_4$ flow rates (<1 $cm^3/s$). The energy available for dissociation to CH radicals and excited carbon species is totally consumed. Consequently, by increasing the power product and the monomer flow, the growth rate can be upgraded (Fig. 8). In addition, a further improvement was achieved by using $C_2H_2$ instead of $CH_4$. This is a consequence of the smaller amount of energy necessary for complete dissociation and ionization of the monomer.

By increasing the chamber pressure, $R_d$ can be upgraded almost linearly (Fig. 9), but there are a few drawbacks. At high $p_c$ (>10 mbar), the radial diffusion of the plasma beam particles is severely restricted, and the beam cross section is reduced to ~1 $cm^2$, decreasing the exposed substrate area. Consequently, the substrate temperature is higher, but the beam is unstable. From Fig. 10, it follows that closer to the nozzle, within practical limitations, even higher growth rates may be achieved. With the addition of hydrogen (Fig. 11), the growth rates are greatly reduced. Appreciable growth rates can be achieved with small amounts of added $H_2$ only with $C_2H_2$ as the feed gas. Because hydrogen addition is necessary to improve the film quality, other parameter settings will have to be studied in the future.

The most relevant results on the growth rate are summarized in Table II.

### *Morphology and Type of Film*

Figures 12 and 13 show SEM micrographs and Raman spectra of films deposited under the divergent conditions of trials 4 and 6 (see Table II). Figure 14 shows some interesting pictures of a film obtained under the conditions of trial 2.

TABLE II

Survey of Deposition Time ($t_d$), Film Thickness ($d_d$), Growth Rate ($R_d$), and Deposited Area ($A_d$) for the Most Relevant Trials

| Trial | Setting | $t_d$ (min) | $d_d$ ($\mu$m) | $R_d$ (nm/s) | $A_d$ ($cm^2$) |
|---|---|---|---|---|---|
| 1 | $[CH_4] = 1$, $p_c = 1$ mbar, $P' = 1$ | 110 | 75 | 11.6 | 30 |
| 2 | $+[CH_4] = 8$ | 30 | 30 | 16.7 | 30 |
| 3 | $+p_c = \frac{8}{3}$ mbar, $P' = \frac{8}{3}$ | 7 | 115 | 274 | 12 |
| 4 | $+p_c = 60$ mbar | 4 | 183 | 762 | 1 |
| 5 | $[C_2H_2] = 8$, $p_c = \frac{8}{3}$ mbar, $P' = \frac{3}{2}$ | 7 | 241 | 574 | 12 |
| 6 | $[C_2H_2] = 3$, $[H_2] = 5$, $p_c = \frac{8}{3}$ mbar, $P' = 1$ | 30 | 133 | 74 | 12 |

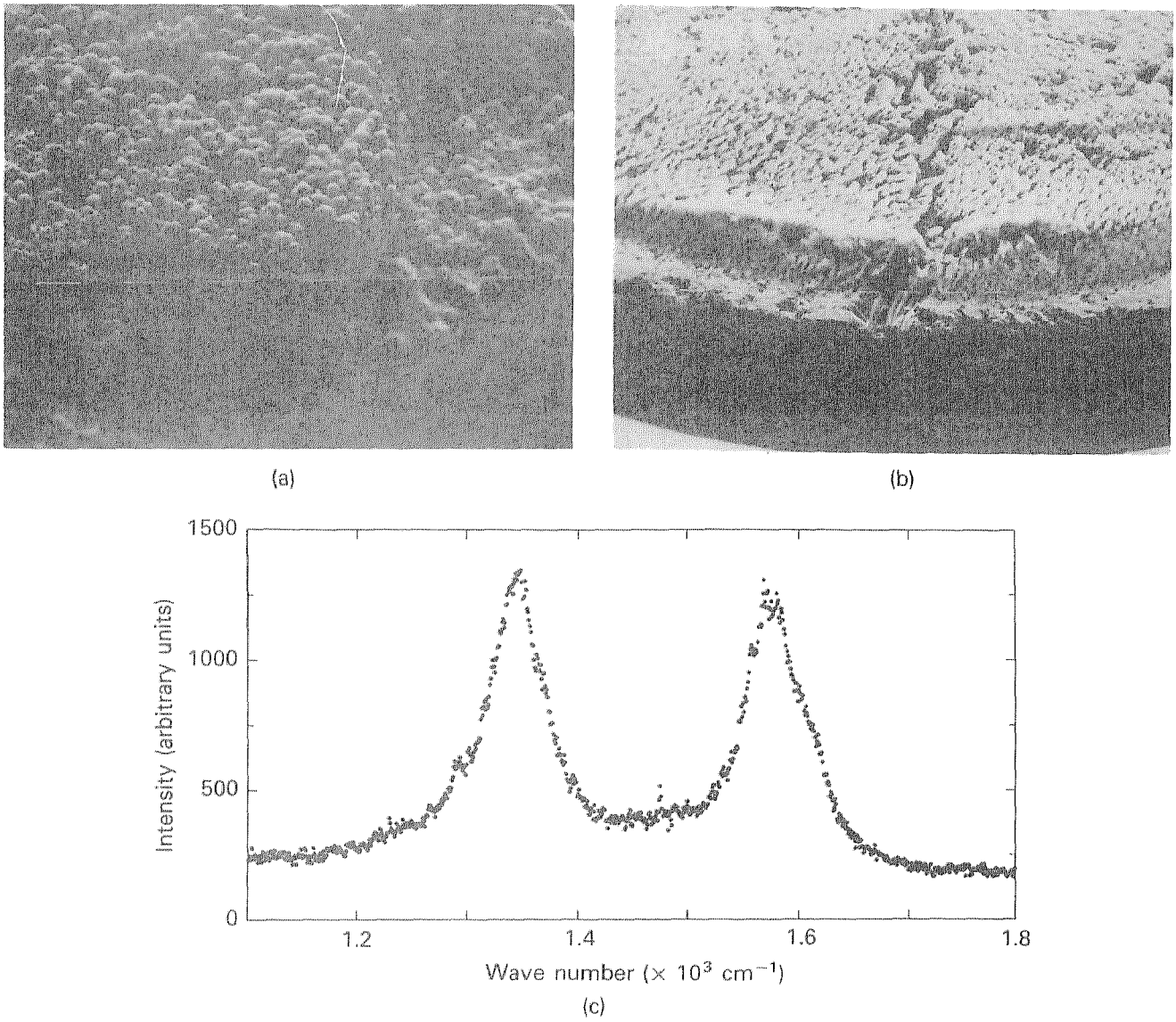


Fig. 12. Film deposited on (a) perpendicular and (b) parallel CFC (1 bar = 10 $\mu$m) and (c) associated Raman spectrum for the perpendicular CFC film: $[CH_4] = 8$, $T_s = 1200°C$, $p_c = 60$ mbar, $P' = \frac{8}{3}$, and $Q' = 3$.

Most of the deposits exhibit a cauliflower morphology, which is similar to that of conventional PyC. In this case, the basal planes of the graphite packets are parallel to the substrate surface.[11] A characterization of the deposits in terms of the random fractal-like structure model as described by Messier and Yehoda[12] is appropriate. The main features of this model are low mobility ($T_{depo} < 0.5T_{melt}$), competitive cone growth, and self-similarity on every dimension of scale. The layers are more continuous on the steel substrate. This may be caused by the lack of preferential sites for nucleation. The sharp edges that can be observed are an indication of the crystalline nature of the deposit.

In all Raman spectra, both the first-order graphite (1581 $cm^{-1}$) and defective graphite peak (1355 $cm^{-1}$) are prominently present. From the intensity ratio of these peaks, a measure for the crystallite size can be estimated.[13] When the peaks are equal in intensity, this size is ~3 nm.

Unfortunately, however, as demonstrated by Figs. 12c and 13c, this is the case for almost all of our films, regardless of the deposition settings. Also no substantial change in Raman spectrum could be observed for the films produced with admixture of low amounts of hydrogen. A broadening of the Raman graphite peaks was observed only for the films deposited at 100°C, indicating a more amorphous film character. Furthermore, the Raman spectra of the films on the steel substrates are very similar to those of the associated films on the CFC substrates. For the films of

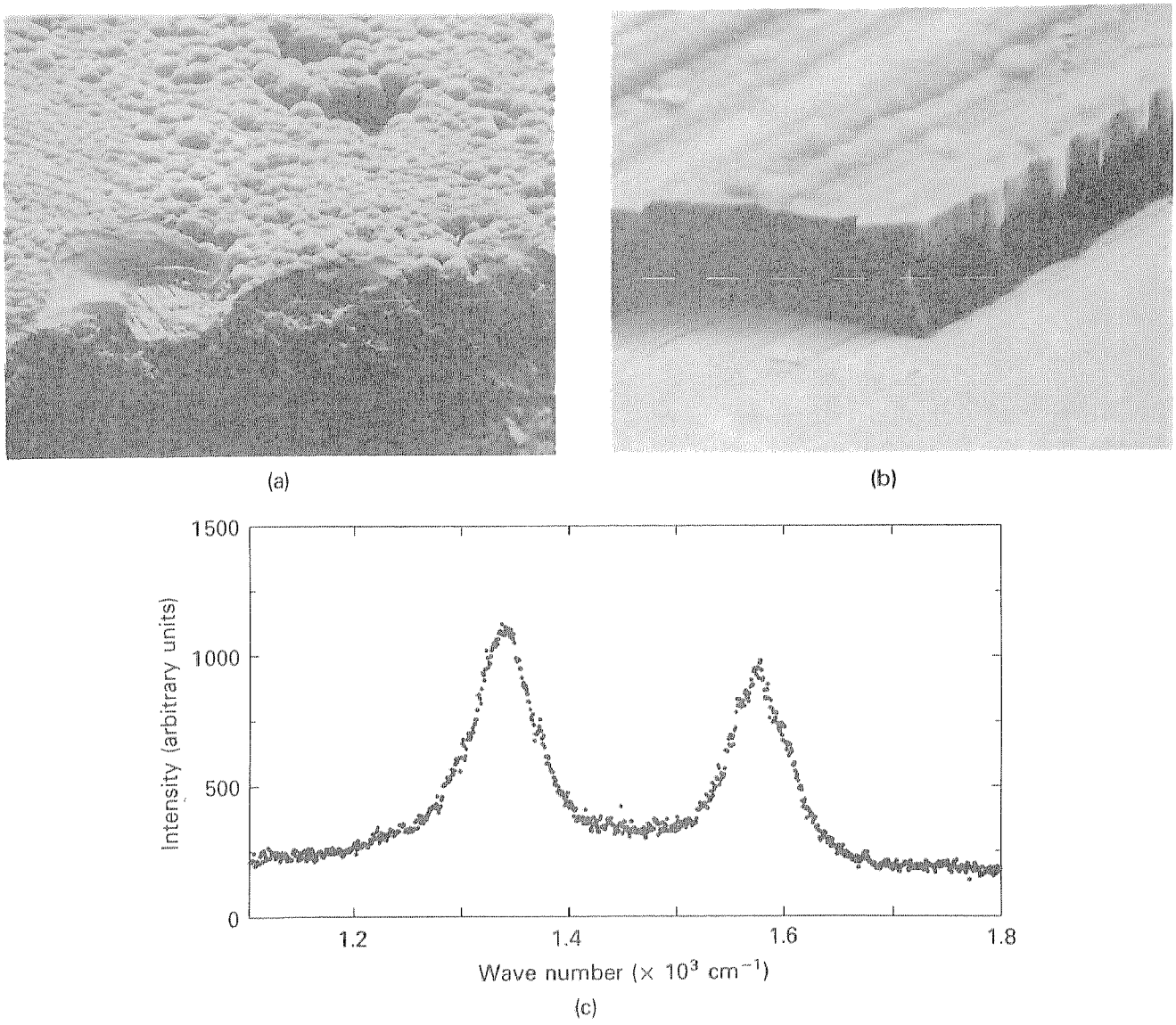


Fig. 13. Film deposited on (a) parallel CFC and (b) steel (1 bar = 10 $\mu$m) and (c) associated Raman spectrum for the parallel CFC film: $[C_2H_2] = 3$, $[H_2] = 5$, H/C = 10/6, $T_s = 700°C$, $p_c = \frac{8}{3}$ mbar, $P' = 1$, and $Q' = 6$.

Fig. 14 on the graphite and the steel substrate, the intensity ratios $I_{1355}/I_{1581}$ amount to 1.30 and 1.25, respectively. Consequently, a more sophisticated analysis of the spectra will be performed in the future. The width of the peaks and their shift with respect to the ideal single crystal values and analysis of the second order peaks will provide additional information.[13]

## CONCLUSIONS

The growth rates obtained without added $H_2$ offer a perspective for further research. Layers that are hundreds of microns thick on an area of ~12 cm$^2$ have been deposited within <30 min. The production of very thick (several millimetres) carbon films within an acceptable period of time (hours) seems to be within the range of possibilities.

The morphology and crystallinity of the deposited film seem to be not very dependent on the deposition parameters, at least in the range used up to now. Most of the films consist of pyrolytic graphite with a crystallite size of ~3 nm and with the basal planes parallel to the substrate surface. In view of the desired thermomechanical qualities of the film, a method for growing films with the basal planes perpendicular to the substrate surface will be sought.

Up to now, the effect of $H_2$ admixture on the film quality could not properly be investigated. With a minor $H_2$ content (<5%) in the flow, no change in crystallite size could be observed. Addition of a substantial

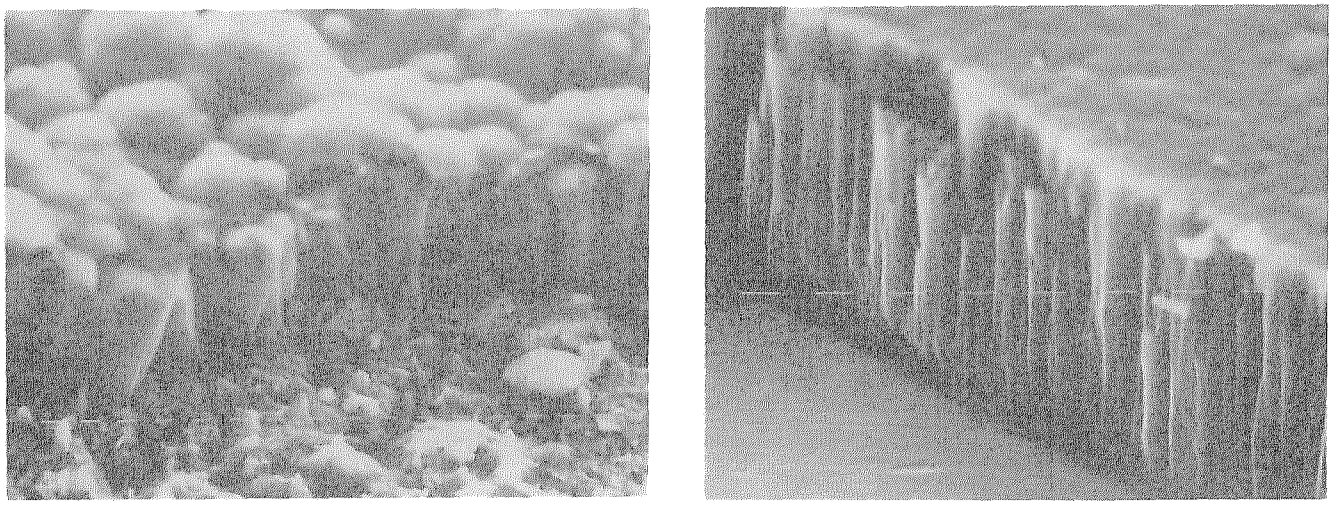

(a) (b)

Fig. 14. Films deposited on (a) commercial graphite and (b) steel: 1 bar = 10 $\mu$m, $[CH_4] = 8$, $T_s \simeq 700°C$, $p_c = 1$ mbar, $P' = 1$, and $Q' = 8$.

amount of hydrogen leads to etching of the graphitic substrates; this shows that deposition is in fact a balance between deposition and etching. The amount of $H_2$ admixture against the arc power may need a very delicate balance in view of optimal ionization and dissociation.

## ACKNOWLEDGMENTS

The authors would like to thank D. J. Stufkens and T. L. Snoeck of the University of Amsterdam for measuring the Raman spectra.

The work reported in the section of graphite deposition in this paper forms part of the NET–ECN Petten–Eindhoven University of Technology research agreement on investigation of plasma-deposited carbon films as a possible means of divertor repair, as established in NET contract 90-237 between the European Atomic Energy Community and Euratom/FOM Association. It is funded by the Commission of the European Communities, which represents the European atomic energy community.

## REFERENCES

1. H. BORNING, "Plasma News Report," Research Institute of Plasma Chemistry and Technology (Sep. 1986).

2. G. M. W. KROESEN, "Plasma Deposition: Investigations on a New Approach," PhD Thesis, Eindhoven University of Technology (1988).

3. H. KERSTEN and G. M. W. KROESEN, "On the Temperature Dependence of the Deposition Rate of Amorphous, Hydrogenated Carbon Films," *J. Vac. Sci. Technol.*, **A8**, *1*, 38 (1990).

4. P. K. BACHMANN et al., "Diamond Deposition from a Cascaded Arc Plasma," *Proc. 3rd Conf. Surface Modification Technologies*, Neuchatel, Switzerland, p. 69 (1989).

5. G. M. W. KROESEN et al., "UV-Visible-IR Spectroscopic Ellipsometer Using a Cascaded Arc as a Light Source" (to be published).

6. G. VIEDER, "ITER Plasma Facing Components," ITER Documentation Series, No. 30, International Atomic Energy Agency (1990).

7. J. J. BEULENS, M. de GRAAF, G. M. W. KROESEN, and D. C. SCHRAM, "Axial Temperatures and Electron Densities in a Flowing Cascaded Arc," *Proc. Materials Research Society Spring Mtg.*, San Francisco, California, April 1990.

8. G. M. W. KROESEN, D. C. SCHRAM, and M. J. F. van de SANDE, "Fast Deposition of Amorphous Hydrogenated Carbon Films Using a Supersonically Expanding Arc Plasma," *Plasma Chem. Plasma Proc.*, **10**, *1*, 49 (1990).

9. J. ROBERTSON, "Amorphous Carbon," *Adv. Phys.*, **35**, *4*, 317 (1986).

10. R. D. WATSON, Ed., "ITER Divertor Engineering Design," ITER-TN-PC-89-1 (Oct. 1989).

11. P. A. THROWER, Ed., "Chemistry and Physics of Carbon: A Series of Advances," Vol. 19, Marcel Dekker, New York (1984).

12. R. MESSIER and J. E. YEHODA, "Geometry of Thin-Film Morphology," *J. Appl. Phys.*, **58**, *10*, 3739 (1985).

13. N. B. BRANDT, S. M. CHUDINOV, and Ya. G. PONOMAREV, *Semimetals: 1. Graphite and Its Compounds*, p. 355, North-Holland, Amsterdam (1988).